

Investigation of the rotational spectrum of CD₃OD and an astronomical search toward IRAS 16293–2422[★]

V. V. Ilyushin¹, H. S. P. Müller², J. K. Jørgensen³, S. Bauerecker⁴, C. Maul⁴, R. Porohovoi¹, E. A. Alekseev¹, O. Dorovskaya¹, F. Lewen², S. Schlemmer², and R. M. Lees⁵

¹ Institute of Radio Astronomy of NASU, Mystetstv 4, 61002 Kharkiv, Ukraine
e-mail: ilyushin@rian.kharkov.ua

² I. Physikalisches Institut, Universität zu Köln, Zùlpicher Str. 77, 50937 Köln, Germany
e-mail: hspm@ph1.uni-koeln.de

³ Niels Bohr Institute, University of Copenhagen, Øster Voldgade 5–7, 1350 Copenhagen K, Denmark

⁴ Institut für Physikalische und Theoretische Chemie, Technische Universität Braunschweig, Gaußstr. 17, 38106 Braunschweig, Germany

⁵ Department of Physics, University of New Brunswick, Saint John, NB E2L 4L5, Canada

Received 06 Jun 2023 / Accepted 26 Jun 2023

ABSTRACT

Solar-type prestellar cores and protostars frequently display large amounts of deuterated organic molecules and, in particular, high relative abundances of doubly and triply deuterated isotopologs. Recent findings on CHD₂OH and CD₃OH toward IRAS 16293–2422 suggest that even fully deuterated methanol, CD₃OD, may be detectable as well. However, searches for CD₃OD are hampered in particular by the lack of intensity information from a spectroscopic model. The objective of the present investigation is to develop a spectroscopic model of CD₃OD in low-lying torsional states that is sufficiently accurate to facilitate searches for this isotopolog in space. We carried out a new measurement campaign for CD₃OD involving two spectroscopic laboratories that covers the 34 GHz–1.1 THz range. A torsion-rotation Hamiltonian model based on the rho-axis method was employed for our analysis. Our resulting model describes the ground and first excited torsional states of CD₃OD well up to quantum numbers $J \leq 51$ and $K_a \leq 23$. We derived a line list for radio-astronomical observations from this model that is accurate up to at least 1.1 THz and should be sufficient for all types of radio-astronomical searches for this methanol isotopolog. This line list was used to search for CD₃OD in data from the Protostellar Interferometric Line Survey of IRAS 16293–2422 obtained with the Atacama Large Millimeter/submillimeter Array. While we found several emission features that can be attributed largely to CD₃OD, their number is still not sufficiently high enough to establish a clear detection. Nevertheless, the estimate of $2 \times 10^{15} \text{ cm}^{-2}$ derived for the CD₃OD column density may be viewed as an upper limit that can be compared to column densities of CD₃OH, CH₃OD, and CH₃OH. The comparison indicates that the CD₃OD column density toward IRAS 16293–2422 is in line with the enhanced D/H ratios observed for multiply deuterated complex organic molecules.

Key words. Molecular data – Methods: laboratory: molecular – Techniques: spectroscopic – Radio lines: ISM – ISM: molecules – Astrochemistry

1. Introduction

Methanol, CH₃OH, is among the most abundant polyatomic molecules in the interstellar medium (ISM) as evidenced by its early radio astronomical detection (Ball et al. 1970). It is observed both in its solid state and gas phase toward star-forming regions (e.g., Herbst & van Dishoeck 2009) and is an important product of the chemistry occurring on the icy surfaces of dust grains (e.g., Tielens & Hagen 1982; Garrod & Herbst 2006). As a slightly asymmetric rotor, whose excitation is strongly dependent on kinetic temperature, methanol presents a useful diagnostic tool for evaluating the physical conditions prevailing in star-forming regions (Leurini et al. 2004). Due to its ubiquity in the ISM, methanol is often taken as a reference for studies of the

chemistry of more complex organic molecules (e.g., Jørgensen et al. 2020).

The ubiquity and high abundance of interstellar methanol make this molecule suitable for studying the degree of deuteration, which is considered as an indicator of the evolution of low-mass star-forming regions (Crapsi et al. 2005; Ceccarelli et al. 2007; Chantzios et al. 2018). Not only has singly deuterated methanol been detected in the ISM, but also doubly and triply deuterated as well. The singly deuterated methanol isotopologs, CH₃OD (Mauersberger et al. 1988) and CH₂DOH (Jacq et al. 1993), were detected first. Some time later, Parise et al. (2002) observed CHD₂OH toward IRAS 16293–2422, followed by Parise et al. (2004) detecting CD₃OH toward the same object. In addition, CHD₂OH was also found toward several other low-mass protostars (Parise et al. 2006; Taquet et al. 2019) and, most recently, in a prestellar core (Lin et al. 2023).

Multiply deuterated isotopic species frequently appear to be overabundant in comparison to the D/H ratio inferred from the singly and non-deuterated species (see e.g., results for doubly deuterated isotopologs of methyl cyanide (CHD₂CN; Cal-

[★] Transition frequencies from this and earlier work are given as supplementary material. We also provide quantum numbers, uncertainties, and residuals between measured frequencies and those calculated from the final set of spectroscopic parameters. The data are available at Centre de Données astronomiques de Strasbourg (CDS) via anonymous ftp to cdsarc.u-strasbg.fr (130.79.128.5) or via <http://cdsweb.u-strasbg.fr/cgi-bin/qcat?J/A+A/>

cutt et al. 2018), methyl formate (CHD₂OCHO; Manigand et al. 2019), and dimethyl ether (CHD₂OCH₃; Richard et al. 2021) toward the low-mass protostellar system IRAS 16293–2422), which may reflect their formation processes at low temperatures (Taquet et al. 2014). Recently revisited abundances of CHD₂OH and CD₃OH toward IRAS 16293–2422 employing the Protostellar Interferometric Line Survey (PILS) data (Drozdovskaya et al. 2022; Ilyushin et al. 2022) also demonstrate this overabundance, suggesting that a search for fully deuterated isotopolog of methanol, CD₃OD, would be promising and timely.

The rotational spectrum of CD₃OD had already been observed in the lab in the 1950s in the context of other methanol isotopologs, in particular, to determine the molecular structure (Venkateswarlu et al. 1955). Lees (1972) published an account of the rotational spectrum of CD₃OD in the microwave region. Additional rotational transition frequencies in the millimeter and/or submillimeter region and with infrared (Mukhopadhyay et al. 2004) or microwave accuracies were reported later (Baskakov & Pashaev 1992; Mukhopadhyay et al. 1998; Xu et al. 2004; Müller et al. 2006). Torsional transition frequencies were provided in two studies very recently (Mukhopadhyay 2021, 2022); these publications also contain some millimeter and submillimeter assignments. The rovibrational spectrum of CD₃OD beyond the torsional manifold was also investigated in some studies, with Lees & Billinghurst (2022) being the most recent one dealing with the COD bending fundamental at 775 cm⁻¹.

The goal of our present investigation is to develop a spectroscopic model of the CD₃OD isotopolog in low-lying torsional states which is sufficiently accurate to provide reliable calculations of line positions and linestrengths for astronomical searches for CD₃OD in the ISM. New measurements were carried out to extend the covered frequency range up to 1.1 THz. The obtained new data were combined with previously published far infrared measurements to form the final dataset involving the rotational quantum numbers up to $J = 51$ and $K = 23$. A fit within experimental error was obtained for the ground and first excited torsional states of the CD₃OD molecule using the so-called rho-axis-method.

We generated a line list that was based on our present results, which we applied in a search for CD₃OD in the Atacama Large Millimeter/submillimeter Array (ALMA) data of the Protostellar Interferometric Line Survey of the deeply embedded protostellar system IRAS 16293–2422 (Jørgensen et al. 2016). While we did not detect CD₃OD confidently, a number of emission lines that can be attributed to CD₃OD (or at least to a large part of it) suggest that a detection is within the reach of ALMA, for instance, by targeting IRAS 16293–2422 through deep observations at lower frequencies – where line confusion may be less problematic.

The rest of the manuscript is organized as follows. Section 2 provides details on our laboratory measurements. The theoretical model, spectroscopic analysis, and fitting results are presented in Sections 3 and 4. Section 5 describes our astronomical observations and the results of our search for CD₃OD, while Section 6 gives the conclusions of our investigation.

2. Experimental details

2.1. Rotational spectra at IRA NASU

The measurements of the CD₃OD spectrum at the Institute of Radio Astronomy (IRA) of NASU were performed in the frequency ranges of 34.5–184 GHz and 234–420 GHz using an automated synthesizer based millimeter wave spectrometer (Ale-

seev et al. 2012). This instrument belongs to a class of absorption spectrometers and uses a set of backward wave oscillators (BWO) to cover the frequency range from 34.5 to 184 GHz, allowing for further extension to the 234–420 GHz range with the help of a solid state tripler from Virginia Diodes, Inc. (VDI). The frequency of the BWO probing signal is stabilized by a two-step frequency multiplication of a reference synthesizer in two phase-lock-loop stages. A commercial sample of CD₃OD was used and all measurements were carried out at room temperature with sample pressures providing linewidths close to the Doppler limited resolution (about 2 Pa). Due to the high rate of D/H exchange at the OH group in CD₃OD, the recorded spectrum contains numerous lines belonging to the CD₃OH isotopolog. These lines do not pose any problem since they may be easily distinguished using the results of our recent study of the CD₃OH spectrum (Ilyushin et al. 2022). Estimated uncertainties for measured line frequencies were 10 kHz, 30 kHz, 50 kHz, and 100 kHz depending on the observed signal-to-noise ratios (S/N).

2.2. Rotational spectra at the Universität zu Köln

The measurements at the Universität zu Köln were carried out at room temperature using a 5 m long single path Pyrex glass cell of 100 mm inner diameter and equipped with high-density polyethylene windows. The cell was filled with 1.5 Pa CD₃OD and refilled after several hours because of the pressure rise due to minute leaks. We utilized three VDI frequency multipliers driven by Rohde & Schwarz SMF 100A synthesizers as sources and a closed cycle liquid He-cooled InSb bolometer (QMC Instruments Ltd) as detector to cover frequencies between 370 and 1095 GHz almost entirely; a small gap near 750 GHz occurred because of a strong water line. Other water lines or low power, especially at the edges, limited the sensitivity in some frequency regions. Frequency modulation was used throughout. The demodulation at $2f$ causes an isolated line to appear close to a second derivative of a Gaussian. Additional information on this spectrometer system is available in Xu et al. (2012). We were able to achieve uncertainties of 5–10 kHz for very symmetric lines with good S/N, as demonstrated in recent studies on excited vibrational lines of CH₃CN (Müller et al. 2021) or on isotopic oxirane (Müller et al. 2022, 2023). Uncertainties of 10 kHz, 30 kHz, 50 kHz, 100 kHz, and 200 kHz were assigned, depending on the observed S/N and on the frequency range.

3. Spectroscopic properties of CD₃OD and our theoretical approach

Fully deuterated methanol, CD₃OD, is a nearly prolate top ($\kappa \approx -0.959$) with a rather high coupling between internal and overall rotations in the molecule ($\rho \approx 0.82$) and the torsional potential barrier V_3 of about 362 cm⁻¹. The torsional problem corresponds to an intermediate barrier case (Lin & Swalen 1959) with the reduced barrier $s = 4V_3/9F \sim 10.9$, where F is the rotation constant of the internal rotor. In comparison with the parent isotopolog, CD₃OD has significantly smaller rotational parameters: $A \approx 2.17$ cm⁻¹, $B \approx 0.630$ cm⁻¹, $C \approx 0.598$ cm⁻¹ in CD₃OD versus $A \approx 4.25$ cm⁻¹, $B \approx 0.823$ cm⁻¹, $C \approx 0.792$ cm⁻¹ in CH₃OH (Xu et al. 2008). Thus, we expect that rotational levels with higher J and K values will be accessible in a room temperature experiment for CD₃OD compared to CH₃OH.

As the theoretical approach in the present study, we employ the so-called rho-axis-method (RAM), which has proven to be the most effective approach so far in treating torsional large

amplitude motions in methanol-like molecules. The method is based on the work of Kirtman (1962), Lees & Baker (1968), and Herbst et al. (1984) and takes its name from the choice of its axis system (Hougen et al. 1994). In the rho-axis-method, the z axis is coincident with the ρ vector, which expresses the coupling between the angular momentum of the internal rotation p_a and that of the global rotation J . We employed the RAM36 code (Ilyushin et al. 2010, 2013) that was successfully used in the past for a number of near prolate tops with rather high ρ and J values (see e.g., Smirnov et al. (2014), Motiyenko et al. (2020), Zakharenko et al. (2019)) and, in particular, for the CD₃OH isotopolog of methanol (Ilyushin et al. 2022). The RAM36 code uses the two-step diagonalization procedure of Herbst et al. (1984) and in the current study, we keep 31 torsional basis functions at the first diagonalization step and 11 torsional basis functions at the second diagonalization step.

The labeling scheme after the second diagonalization step is based on an eigenfunction composition but, in contrast to our CD₃OH study (Ilyushin et al. 2022), is not limited to searching for a dominant eigenvector component only. Since methanol is a nearly symmetric prolate top ($\kappa \approx -0.98$), in which the angle between the RAM a -axis and the principal-axis-method (PAM) a -axis is only 0.07° , it is assumed that the RAM a -axis in methanol is suitable for K quantization and that eigenvectors can be unambiguously assigned using dominant components. And indeed, searching for a dominant eigenvector component worked well in the case of the CD₃OH isotopolog (Ilyushin et al. 2022), for which the angle between the RAM a -axis and the PAM a -axis is only 0.14° and the asymmetry parameter ($\kappa \approx -0.977$) is nearly the same as in CH₃OH ($\kappa \approx -0.982$). In CD₃OD, however, the angle between the RAM a -axis and PAM a -axis is 0.68° and $\kappa \approx -0.959$, and it appeared that starting from $J \approx 25$, some eigenvectors do not have a dominant eigenvector component that would allow for unambiguous labeling. Therefore, we have employed a combined labeling scheme. First, we search for a dominant eigenvector component (≥ 0.8) and if it exists, the level is labeled according to this dominant component. If such component is absent then we search for similarities in basis-set composition in torsion-rotation eigenvectors belonging to the previous J value and assign the level according to the highest degree of similarity found. The general idea assumes that for a given pair of K_a, v_t values, the torsion-rotation eigenfunctions vary slowly when J changes by one, and this slow change should appear as a high degree of similarity in the eigenvector compositions of the states corresponding to the same K_a, v_t , and adjacent J values. This approach allows one to transfer a given K_a -label from lower J values, where it can be determined easily (either from eigenvector composition using dominant component or from energy-ordering considerations), to higher J values, which are characterized by extensive basis-set mixing. The details of this approach to K -labeling for torsion-rotation energy levels in low-barrier molecules can be found in Ilyushin (2004).

The energy levels are labeled in our fits and predictions by the free rotor quantum number, m , the overall rotational angular momentum quantum number, J , and a signed value of K_a , which is the axial a -component of the overall rotational angular momentum, J . In the case of the A symmetry species, the $+/-$ sign corresponds to the so-called "parity" designation, which is related to the A1/A2 symmetry species in the group G_6 (Hougen et al. 1994). The signed value of K_a for the E symmetry species reflects the fact that the Coriolis-type interaction between the internal rotation and the global rotation causes the $|K_a| > 0$ levels to split into a $K_a > 0$ level and a $K_a < 0$ level. We also provide K_c values for convenience, but they are simply recalculated from

the J and K_a values, $K_c = J - |K_a|$ for $K_a \geq 0$ and $K_c = J - |K_a| + 1$ for $K_a < 0$. The m values 0, $-3, 3 / 1, -2, 4$ correspond to A/E transitions of the $v_t = 0, 1$, and 2 torsional states, respectively.

4. Spectroscopic results

We started our analysis from the results of Müller et al. (2006), where the dataset, consisting of 488 $v_t = 0$ and 182 $v_t = 1$ microwave transitions, ranging up to $J_{\max} = 25$ and $K_{\max} = 14$, was fit with 56 parameters of the RAM Hamiltonian, and a weighted standard deviation of 3.13 was achieved. Since the BELGI code (Kleiner 2010) was used in the previous study (Müller et al. 2006), we refit the available dataset with the RAM36 program (Ilyushin et al. 2010, 2013) as the first step. The resulting fit was the starting point of our present analysis.

New data were assigned starting with the Kharkiv measurements. First, the search for the $v_t = 2$ rotational transitions was performed with success, and further assignments were made in parallel for the three torsional states of CD₃OD $v_t = 0, 1$, and 2. Submillimeter wave and THz measurements from Cologne were assigned subsequently, based on our new results. Whenever it was possible, we replaced the old measurements from Müller et al. (2006) and references therein with the more accurate new ones. At the same time, we decided to keep in the fits two measured values for the same transition from the Kharkiv and Cologne spectral recordings in that part of the frequency range where the measurements from the two laboratories overlap (370–420 GHz). A rather good agreement within the experimental uncertainties was observed for this limited set of duplicate new measurements. Finally, at an advanced stage of our analysis, the FIR data from Mukhopadhyay (2021) were added to the fit.

The assignment process was performed in a usual bootstrap manner, with numerous cycles of refinement of the parameter set while the new data were gradually added. In parallel, a search of the optimal set of RAM torsion-rotation parameters was carried out, and it finally became evident that the $v_t = 2$ torsional state poses some problems with fitting. The strong influence of inter-vibrational interactions arising from low lying small amplitude vibrations in CD₃OD, which then propagate down through numerous intertorsional interactions, is a possible explanation for these problems. We encountered similar problems with CD₃OH (Ilyushin et al. 2022). There we decided to limit our fitting attempts mainly to the ground and first excited torsional states. Taking into account that one of our goals was to provide reliable predictions for astrophysical searches of interstellar CD₃OD, we adopted an analogous decision in the current case of the CD₃OD investigation. Thus, at the final stage of model refinement, we limited our fitting attempts mainly to the ground and first excited torsional states of CD₃OD. Only the lowest three K series for the A and E species in $v_t = 2$ were retained in the fits in order to get a better constraint of the torsional parameters in the Hamiltonian model. These $v_t = 2$ K levels should be affected least by the intervibrational interactions arising from low lying small amplitude vibrations. In the case of CD₃OD, this corresponds to $K = -1, 2, 3$ for the E species in $v_t = 2$ and to $K = -4, 0, 4$ for the A species.

It should be noted that at the final stage of preparation of this manuscript, the new study of Mukhopadhyay (2022) appeared. This study emphasized the transitions involving the second excited torsional state levels. Taking into account that our efforts are essentially concentrated on the ground and first excited torsional states of CD₃OD, we decided not to include any data from Mukhopadhyay (2022) in the present analysis even

those involving the lowest three K series of levels for the A and E species in $v_t = 2$, which were retained in the fits otherwise. Submillimeter wave transitions appeared from Mukhopadhyay (2022) were also not included in our present fits since they are within the range of our current measurements, with our measurements being more precise. We intend to include the data from Mukhopadhyay (2022) at the next stage of our investigation of CD₃OD, when we will try to fit transition higher in v_t and try to model the intervibrational interactions arising from low lying small amplitude vibrations in CD₃OD. With this aim in mind, new measurements of the CD₃OD IR spectrum between 500 and 1200 cm⁻¹ were carried out at the Technische Universität Braunschweig, which we plan to consider in our future analyses of the CD₃OD spectrum.

Our final CD₃OD dataset for the purposes of this paper involves 4337 FIR and 10001 microwave line frequencies that correspond, due to blending, to 16259 transitions with $J_{\max} = 51$. Due to the duplication in measurements mentioned above, the number of unique transitions incorporated in the fit is somewhat lower at 15135. A Hamiltonian model consisting of 117 parameters provided a fit with a weighted root mean square (RMS) deviation of 0.71 which was selected as our "best fit" for this paper. The 117 molecular parameters from our final fit are given in Table A.1 (Appendix A). The numbers of the terms in the model distributed between the orders $n_{\text{op}} = 2, 4, 6, 8, 10, 12$ are 7, 22, 45, 34, 8, and 1 respectively, which is consistent with the limits of determinable parameters of 7, 22, 50, 95, 161, and 252 for these orders, as calculated from the differences between the total number of symmetry-allowed Hamiltonian terms of order n_{op} and the number of symmetry-allowed contact transformation terms of order $n_{\text{op}} - 1$, when applying the ordering scheme of Nakagawa et al. (1987). The final set of the parameters converged perfectly in all three senses: (i) the relative change in the weighted RMS deviation of the fit at the last iteration was about $\sim 10^{-7}$; (ii) the corrections to the parameter values generated at the last iteration are less than $\sim 10^{-3}$ of the calculated parameter confidence intervals; and (iii) the changes generated at the last iteration in the calculated frequencies are less than 1 kHz even for the FIR data.

A summary of the quality of this fit is given in Table 1. The overall weighted RMS deviation of 0.71 and the additional fact that all data groups are fit within experimental uncertainties (see the left part of Table 1 where the data are grouped by measurement uncertainty) seems satisfactory to us. If we consider the weighted RMS deviations for the data grouped by torsional state we will see a rather good agreement between our model and the experiment for all three torsional states as well as for the torsional fundamental band. Further illustration of our current understanding of the microwave spectrum of CD₃OD may be found at Figs. 1 and 2. It is seen that our current model reproduces the observed microwave spectrum quite well both with respect to line positions and line intensities.

Using the parameters of our final fit we calculated a list of CD₃OD transitions in the ground and first excited torsional states for astronomical observations. The dipole moment function of Mekhtiev et al. (1999) was employed in our calculations where the values for the permanent dipole moment components of CH₃OH were replaced by appropriate ones for CD₃OD $\mu_a = 0.867$ D and $\mu_b = 1.430$ D taken from Mukhopadhyay et al. (1998). The permanent dipole moment components were rotated from the principal axis system to the rho axis system of our Hamiltonian model. As in the case of CD₃OH (Ilyushin et al. 2022), the list of CD₃OD transitions includes information on transition quantum numbers, transition frequencies, calculated

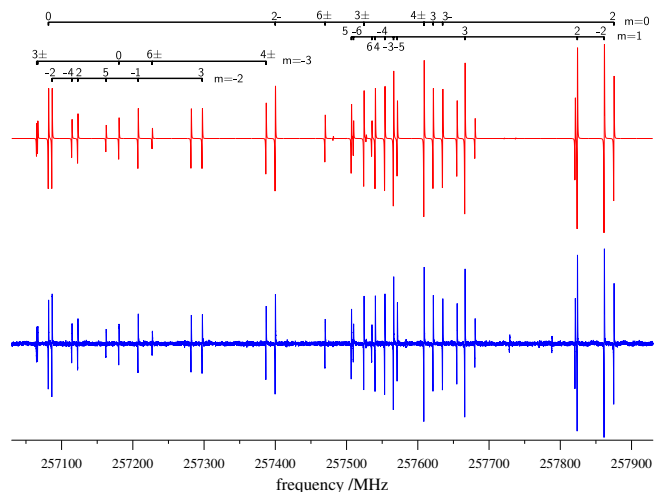


Fig. 1. Portion of the CD₃OD microwave spectrum dominated by $J = 7 \leftarrow 6$ R-branch of transitions in the 257.03–257.93 GHz range. The observed spectrum is shown in the lower panel and the calculated one in the upper one. The K quantum numbers for the $m = 0, 1$ ($v_t = 0$) and $m = -2, -3$ ($v_t = 1$) $J = 7 \leftarrow 6$ transitions are given at the top. It is seen that the experimental frequencies and the intensity pattern are rather well reproduced by our model for the spectral features dominating this frequency range.

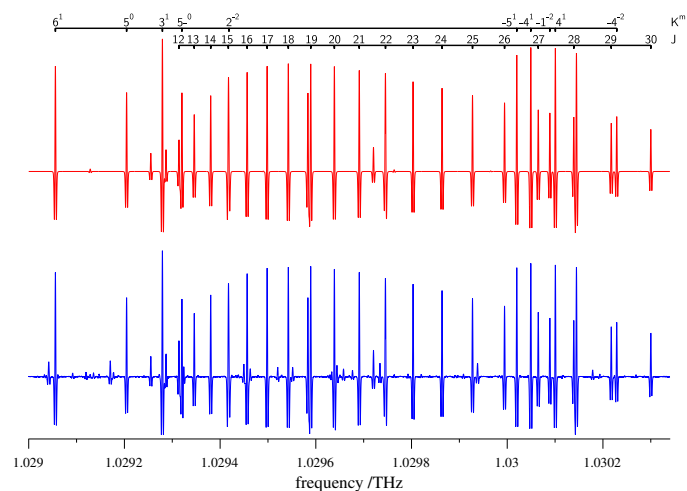


Fig. 2. Portion of the CD₃OD THz spectrum dominated by $m = 1$ $K = -12 \leftarrow -11$ Q-branch and $J = 28 \leftarrow 27$ R-branch transitions in the 1.029–1.030 THz range. The observed spectrum is shown in the lower panel and the calculated one in the upper one. The J quantum numbers for the $m = 1$ $K = -12 \leftarrow -11$ Q-branch and the K and m quantum numbers (K^m) for the $J = 28 \leftarrow 27$ R-branch are given at the top. It is seen that the experimental frequencies and the intensity pattern are rather well reproduced by our model for the spectral features dominating this frequency range.

uncertainties, lower state energies, and transition strengths. To avoid unreliable extrapolations far beyond the quantum number coverage of the available experimental dataset, we limited our predictions by $v_t \leq 1$, $J \leq 55$ and $|K_a| \leq 25$. As already mentioned earlier, we label torsion-rotation levels by the free rotor quantum number, m , the overall rotational angular momentum quantum number, J , a signed value of K_a , and K_c . The calculations were done up to 1.33 THz. Additionally, we limit our calculations to transitions for which calculated uncertainties are less than 0.1 MHz. The lower state energies are given referenced

to the $K_a = 0$ A-type $v_t = 0$ level. We provide additionally the torsion-rotation part of the partition function $Q_{rt}(T)$ of CD₃OD calculated from first principles, that is, via direct summation over the torsion-rotational states. The maximum J value is 90 and $n_{v_t} = 11$ torsional states were taken into account. The calculations, as well as the experimental line list from the present work, can be found in the online Supplementary material with this article and will also be available in the Cologne Database for Molecular Spectroscopy, (CDMS, Endres et al. 2016).

5. Astronomical search for CD₃OD

The new spectroscopic calculations were used to search for CD₃OD in data from the Protostellar Interferometric Line Survey (PILS; Jørgensen et al. 2016). PILS represents an unbiased spectral survey of the Class 0 protostellar system IRAS 16293–2422 using the Atacama Large Millimeter/submillimeter Array covering the frequency range from 329 to 363 GHz. The data cover the region of IRAS 16293–2422 including its two primary components “A” and “B” that show abundant lines of complex organic molecules at an angular resolution of $\sim 0.5''$ and a spectral resolution of ~ 0.2 km s⁻¹. Toward a position slightly offset from the “B” component of the system, the lines are intrinsically narrow, making it an ideal hunting ground for new species and several complex organic molecules and their isotopologs have been identified there, including other deuterated isotopologs of CH₃OH such as CH₂DOH and CH₃OD (Jørgensen et al. 2018), CHD₂OH (Drozdovskaya et al. 2022), and CD₃OH (Ilyushin et al. 2022).

The search for CD₃OD was conducted following the approach applied in other papers from PILS: synthetic spectra are calculated assuming that the excitation of the molecule is characterized by local thermodynamical equilibrium, which is reasonable at the densities on the scales probed by PILS (Jørgensen et al. 2016). The source velocity offset relative to the local standard of rest is assumed to be 2.6 km s⁻¹ and the line full width at half maximum (FWHM) is taken as 1 km s⁻¹. With these assumptions the kinetic temperature and column density of the species are left as the two free parameters. For the search we assume a temperature of 225 K similar to that of CD₃OH (Ilyushin et al. 2022). Figure 3 shows the 16 lines predicted to be strongest for this temperature: the column density is taken to be the maximum possible without overproducing lines compared to the RMS noise level of the data with a value of 2×10^{15} cm⁻². As we can see, three to four lines match the observed spectral features at or slightly above the 3σ level in the data. One line at 348.988 GHz is predicted at the 3σ level but does not show any observed emission. However, that one is overlapping with the absorption part of a nearby, stronger, transition so that may not be significant. The quoted column density would correspond to an CD₃OD abundance of 0.02% relative to the main isotopolog CH₃OH (the column density of that constrained by observations of optically thin transitions of CH₃¹⁸OH). If all D/H substitutions would be considered equally probable, this in turn would imply a D/H ratio of about 12% – similar to what is measured for other multiple deuterated species and enhanced relative to the ratios measured from the singly deuterated variants (CH₂DOH and CH₃OD). While this makes the assignments of the three to four transitions plausible it is not possible to claim a solid detection based on so few lines. However, the analysis demonstrates that the detection of CD₃OD is within the reach of ALMA, for instance, by targeting IRAS 16293–2422 through deep observations at lower frequencies where line confusion may be less problematic.

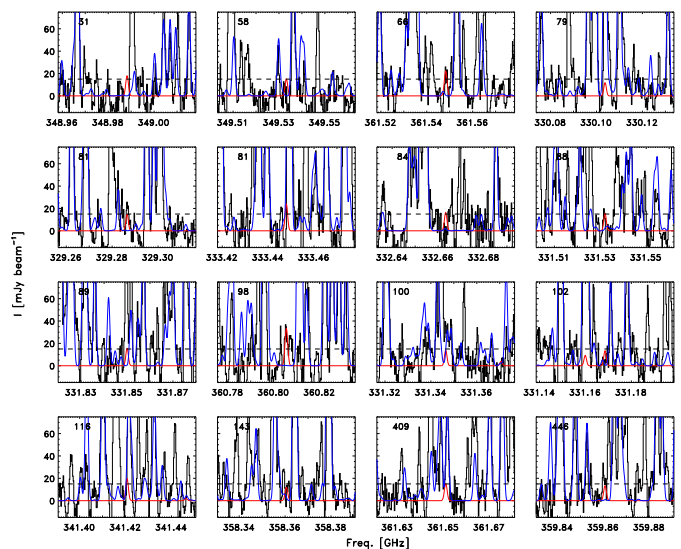


Fig. 3. Sixteen lines predicted to be the strongest toward the position offset by 1 beam ($0.5''$) from IRAS16293B: the observations are shown in the black, the synthetic spectrum for CD₃OD in red, and other species identified as part of PILS in blue. The dashed line indicates the 3σ RMS level of the data per 1 km s⁻¹ (1 km s⁻¹ is the typical FWHM line width of the lines toward this position).

6. Conclusion

In this work, we performed a new study of the torsion-rotation spectrum of the CD₃OD isotopolog using a torsion-rotation RAM Hamiltonian. The new microwave measurements carried out in the broad frequency range from 34.5 GHz to 1.1 THz and transitions with J up to 51 and K_a up to 23 involving the $v_t = 0$, 1, 2 torsional states were assigned and analyzed. After revealing perturbations in the second excited torsional state of CD₃OD, presumably caused by the intervibrational interactions arising from low-lying small-amplitude vibrations in this molecule, we concentrated our efforts on refining the theoretical model for the ground and first excited torsional states only. A fit within the experimental uncertainties (weighted RMS deviation 0.71) was achieved for the dataset consisting of 4337 FIR and 10001 microwave line frequencies.

Based on our results, calculations of the ground and first excited torsional states were carried out and used in a search for CD₃OD spectral features in data from the ALMA PILS survey of the deeply embedded protostar IRAS 16293–2422. While three to four CD₃OD transitions match observed spectral features at or slightly above the 3σ level in the data, it is not possible to claim a solid detection based on so few lines. Nevertheless, our analysis demonstrates that the detection of CD₃OD in IRAS 16293–2422 using ALMA is quite probable through deep observations at lower frequencies where line confusion may be less problematic. The upper column density limit of 2×10^{15} cm⁻² for CD₃OD was derived based on the assumption of an excitation temperature of 225 K (taken similar to that of CD₃OH (Ilyushin et al. 2022)). Comparison with the CH₃OH main isotopolog (for which the column density is deduced from optically thin lines of CH₃¹⁸OH) yields a CD₃OD/CH₃OH ratio as high as $\sim 0.02\%$, thus implying that the fully deuterated methanol is in line with the enhanced D/H ratios observed for multiply deuterated complex organic molecules.

Acknowledgements. We acknowledge support by the Deutsche Forschungsgemeinschaft via the collaborative research center SFB 956 (project ID 184018867)

project B3 as well as the Gerätezentrum SCHL 341/15-1 (“Cologne Center for Terahertz Spectroscopy”). The research in Kharkiv and Braunschweig was carried out under support of the Volkswagen foundation. The assistance of the Science and Technology Center in the Ukraine is acknowledged (STCU partner project P756). J.K.J. is supported by the Independent Research Fund Denmark (grant number 0135-00123B). R.M.L. received support from the Natural Sciences and Engineering Research Council of Canada. Our research benefited from NASA’s Astrophysics Data System (ADS). This paper makes use of the following ALMA data: ADS/JAO.ALMA # 2013.1.00278.S. ALMA is a partnership of ESO (representing its member states), NSF (USA) and NINS (Japan), together with NRC (Canada), MOST and ASIAA (Taiwan), and KASI (Republic of Korea), in cooperation with the Republic of Chile. The Joint ALMA Observatory is operated by ESO, AUI/NRAO and NAOJ.

References

- Alekseev, E. A., Motiyenko, R. A., & Margules, L. 2012, *Radio Phys. Radio Astron.*, 3, 75
- Ball, J. A., Gottlieb, C. A., Lilley, A. E., & Radford, H. E. 1970, *ApJ*, 162, L203
- Baskakov, O. I. & Pashaev, M. A. O. 1992, *J. Mol. Spectrosc.*, 151, 282
- Calcutt, H., Jørgensen, J. K., Müller, H. S. P., et al. 2018, *A&A*, 616, A90
- Ceccarelli, C., Caselli, P., Herbst, E., Tielens, A. G. G. M., & Caux, E. 2007, in *Protostars and Planets V*, ed. B. Reipurth, D. Jewitt, & K. Keil, 47
- Chantzos, J., Spezzano, S., Caselli, P., et al. 2018, *ApJ*, 863, 126
- Crapsi, A., Caselli, P., Walmsley, C. M., et al. 2005, *ApJ*, 619, 379
- Drozdovskaya, M. N., Coudert, L. H., Margulès, L., et al. 2022, *A&A*, 659, A69
- Endres, C. P., Schlemmer, S., Schilke, P., Stutzki, J., & Müller, H. S. P. 2016, *J. Mol. Spectrosc.*, 327, 95
- Garrod, R. T. & Herbst, E. 2006, *A&A*, 457, 927
- Herbst, E., Messer, J. K., DeLucia, F. C., & Helminger, P. 1984, *J. Mol. Spectrosc.*, 108, 42
- Herbst, E. & van Dishoeck, E. F. 2009, *ARA&A*, 47, 427
- Hougen, J. T., Kleiner, I., & Godefroid, M. 1994, *J. Mol. Spectrosc.*, 163, 559
- Ilyushin, V. 2004, *J. Mol. Spectrosc.*, 227, 140
- Ilyushin, V. V., Endres, C. P., Lewen, F., Schlemmer, S., & Drouin, B. J. 2013, *J. Mol. Spectrosc.*, 290, 31
- Ilyushin, V. V., Kisiel, Z., Pszczókowski, L., Mäder, H., & Hougen, J. T. 2010, *J. Mol. Spectrosc.*, 259, 26
- Ilyushin, V. V., Müller, H. S. P., Jørgensen, J. K., et al. 2022, *A&A*, 658, A127
- Jacq, T., Walmsley, C. M., Mauersberger, R., et al. 1993, *A&A*, 271, 276
- Jørgensen, J. K., Belloche, A., & Garrod, R. T. 2020, *ARA&A*, 58, 727
- Jørgensen, J. K., Müller, H. S. P., Calcutt, H., et al. 2018, *A&A*, 620, A170
- Jørgensen, J. K., van der Wiel, M. H. D., Coutens, A., et al. 2016, *A&A*, 595, A117
- Kirtman, B. 1962, *J. Chem. Phys.*, 37, 2516
- Kleiner, I. 2010, *J. Mol. Spectrosc.*, 260, 1
- Lees, R. M. 1972, *J. Chem. Phys.*, 56, 5887
- Lees, R. M. & Baker, J. G. 1968, *J. Chem. Phys.*, 48, 5299
- Lees, R. M. & Billinghurst, B. E. 2022, *J. Mol. Spectrosc.*, 384, 111592
- Leurini, S., Schilke, P., Menten, K. M., et al. 2004, *A&A*, 422, 573
- Lin, C. C. & Swalen, J. D. 1959, *Rev. Mod. Phys.*, 31, 841
- Lin, Y., Spezzano, S., & Caselli, P. 2023, *A&A*, 669, L6
- Manigand, S., Calcutt, H., Jørgensen, J. K., et al. 2019, *A&A*, 623, A69
- Mauersberger, R., Henkel, C., Jacq, T., & Walmsley, C. M. 1988, *A&A*, 194, L1
- Mekhtiev, M. A., Godfrey, P. D., & Hougen, J. T. 1999, *J. Mol. Spectrosc.*, 194, 171
- Motiyenko, R., Ilyushin, V., Demaison, J., et al. 2020, *J. Mol. Struct.*, 1213, 128037
- Mukhopadhyay, I. 2021, *Infrared Phys. Technol.*, 114, 103668
- Mukhopadhyay, I. 2022, *Infrared Phys. Technol.*, 125, 104298
- Mukhopadhyay, I., Duan, Y.-B., & Klee, S. 2004, *J. Mol. Struct.*, 695-696, 367
- Mukhopadhyay, I., Sastry, K. V. L. N., & Winniewisser, M. 1998, *Spectrochim. Acta A*, 54, 1375
- Mukhopadhyay, I., Sudhakaran, G., & Mellau, G. 1998, *Spectrochim. Acta A*, 54, 1307
- Müller, H. S. P., Belloche, A., Lewen, F., et al. 2021, *J. Mol. Spectrosc.*, 378, 111449
- Müller, H. S. P., Guillemin, J.-C., Lewen, F., & Schlemmer, S. 2022, *J. Mol. Spectrosc.*, 384, 111584
- Müller, H. S. P., Jørgensen, J. K., Guillemin, J.-C., Lewen, F., & Schlemmer, S. 2023, *MNRAS*, 518, 185
- Müller, H. S. P., Xu, L.-H., & van der Tak, F. 2006, *J. Mol. Struct.*, 795, 114
- Nakagawa, K., Tsunekawa, S., & Kojima, T. 1987, *J. Mol. Spectrosc.*, 126, 329
- Parise, B., Castets, A., Herbst, E., et al. 2004, *A&A*, 416, 159
- Parise, B., Ceccarelli, C., Tielens, A. G. G. M., et al. 2006, *A&A*, 453, 949
- Parise, B., Ceccarelli, C., Tielens, A. G. G. M., et al. 2002, *A&A*, 393, L49
- Richard, C., Jørgensen, J. K., Margulès, L., et al. 2021, *A&A*, 651, A120
- Smirnov, I. A., Alekseev, E. A., Ilyushin, V. V., et al. 2014, *J. Mol. Spectrosc.*, 295, 44
- Taquet, V., Bianchi, E., Codella, C., et al. 2019, *A&A*, 632, A19
- Taquet, V., Charnley, S. B., & Sipilä, O. 2014, *ApJ*, 791, 1
- Tielens, A. G. G. M. & Hagen, W. 1982, *A&A*, 114, 245
- Venkateswarlu, P., Edwards, H. D., & Gordy, W. 1955, *J. Chem. Phys.*, 23, 1195
- Xu, L.-H., Fisher, J., Lees, R. M., et al. 2008, *J. Mol. Spectrosc.*, 251, 305
- Xu, L.-H., Lees, R. M., Crabbe, G. T., et al. 2012, *J. Chem. Phys.*, 137, 104313
- Xu, L. H., Müller, H. S. P., van der Tak, F. F. S., & Thorwirth, S. 2004, *J. Mol. Spectrosc.*, 228, 220
- Zakharenko, O., Ilyushin, V. V., Lewen, F., et al. 2019, *A&A*, 629, A73

Table 1. Overview of the dataset and the fit quality

By measurement uncertainty			By torsional state		
Unc. ^a	# ^b	RMS ^c	v_t^d	# ^b	WRMS ^e
0.010 MHz	3734	0.0088 MHz	$v_t = 0 \leftarrow 0$	8138	0.69
0.020 MHz	116	0.0110 MHz	$v_t = 1 \leftarrow 1$	5832	0.84
0.030 MHz	4335	0.0223 MHz	$v_t = 2 \leftarrow 2$	165	0.81
0.040 MHz	6	0.0177 MHz	$v_t = 1 \leftarrow 0$	2124	0.36
0.050 MHz	588	0.0461 MHz			
0.100 MHz	1109	0.0779 MHz			
0.200 MHz	113	0.1662 MHz			
$5 \times 10^{-4} \text{ cm}^{-1}$	4337	$2.0 \times 10^{-4} \text{ cm}^{-1}$			

Notes. ^a Estimated measurement uncertainties for each data group. ^b Number of lines (left part) or transitions (right part) of each category in the least-squares fit. Note that due to blending 14338 measured line frequencies correspond to 16259 transitions in the fit, which in turn due to presence of duplicate measurements represent 15135 unique transitions in the fit. ^c Root-mean-square (RMS) deviation of corresponding data group. ^d Upper and lower state torsional quantum number v_t . ^e Weighted root-mean-square (WRMS) deviation of corresponding data group.

Appendix A: Parameters of the RAM Hamiltonian for the CD₃OD moleculeTable A.1. Fitted parameters of the RAM Hamiltonian for the CD₃OD molecule

n_{tr}^a	Operator ^b	Par. ^c	Value ^{d,e}
2 _{2,0}	$(1 - \cos 3\alpha)$	$(1/2)V_3$	181.1021642(55)
2 _{2,0}	P_a^2	F	14.75939375(90)
2 _{1,1}	$P_a P_\alpha$	ρ	0.8219648943(19)
2 _{0,2}	P_a^2	A	2.1693625(90)
2 _{0,2}	P_b^2	B	0.63055239(26)
2 _{0,2}	P_c^2	C	0.59843413(22)
2 _{0,2}	$(1/2)\{P_a, P_b\}$	$2D_{ab}$	0.03656819(19)
4 _{4,0}	$(1 - \cos 6\alpha)$	$(1/2)V_6$	-1.076539(13)
4 _{4,0}	P_a^4	F_m	$-0.2905843(26) \times 10^{-2}$
4 _{3,1}	$P_a P_\alpha^3$	ρ_m	$-0.11365193(86) \times 10^{-1}$
4 _{2,2}	$P^2(1 - \cos 3\alpha)$	V_{3J}	$-0.1682007(47) \times 10^{-2}$
4 _{2,2}	$P_a^2(1 - \cos 3\alpha)$	V_{3K}	$0.66900(17) \times 10^{-2}$
4 _{2,2}	$(P_b^2 - P_c^2)(1 - \cos 3\alpha)$	V_{3bc}	$0.6739(49) \times 10^{-5}$
4 _{2,2}	$(1/2)\{P_a, P_b\}(1 - \cos 3\alpha)$	V_{3ab}	$0.12557689(93) \times 10^{-1}$
4 _{2,2}	$P^2 P_a^2$	F_J	$-0.5466106(39) \times 10^{-4}$
4 _{2,2}	$P_a^2 P_\alpha^2$	F_K	$-0.1678373(11) \times 10^{-1}$
4 _{2,2}	$(P_b^2 - P_c^2) P_\alpha^2$	F_{bc}	$-0.106428(57) \times 10^{-3}$
4 _{2,2}	$(1/2)\{P_a, P_c\} \sin 3\alpha$	D_{3ac}	$0.1808855(27) \times 10^{-1}$
4 _{2,2}	$(1/2)\{P_b, P_c\} \sin 3\alpha$	D_{3bc}	$-0.8227(13) \times 10^{-3}$
4 _{1,3}	$P^2 P_a P_\alpha$	ρ_J	$-0.8252990(66) \times 10^{-4}$
4 _{1,3}	$P_a^3 P_\alpha$	ρ_K	$-0.11023649(58) \times 10^{-1}$
4 _{1,3}	$(1/2)\{P_a, (P_b^2 - P_c^2)\} P_\alpha$	ρ_{bc}	$-0.151933(58) \times 10^{-3}$
4 _{1,3}	$(1/2)\{P_a^2, P_b\} P_\alpha$	ρ_{ab}	$-0.22531(72) \times 10^{-5}$
4 _{0,4}	P^4	$-\Delta_J$	$-0.8557802(47) \times 10^{-6}$
4 _{0,4}	$P^2 P_a^2$	$-\Delta_{JK}$	$-0.3430628(28) \times 10^{-4}$
4 _{0,4}	P_a^4	$-\Delta_K$	$-0.2715830(13) \times 10^{-2}$
4 _{0,4}	$P^2(P_b^2 - P_c^2)$	$-2\delta_J$	$-0.954346(64) \times 10^{-7}$
4 _{0,4}	$(1/2)\{P_a^2, (P_b^2 - P_c^2)\}$	$-2\delta_K$	$-0.497826(92) \times 10^{-4}$
4 _{0,4}	$(1/2)P^2\{P_a, P_b\}$	D_{abJ}	$-0.48978(15) \times 10^{-6}$
6 _{6,0}	P_a^6	F_{mm}	$0.21266(57) \times 10^{-5}$
6 _{5,1}	$P_a P_\alpha^5$	ρ_{mm}	$0.13678(28) \times 10^{-4}$
6 _{4,2}	$P^2(1 - \cos 6\alpha)$	V_{6J}	$-0.835(18) \times 10^{-5}$
6 _{4,2}	$P_a^2(1 - \cos 6\alpha)$	V_{6K}	$-0.1930(66) \times 10^{-3}$
6 _{4,2}	$(P_b^2 - P_c^2)(1 - \cos 6\alpha)$	V_{6bc}	$-0.31339(65) \times 10^{-4}$
6 _{4,2}	$P^2 P_a^4$	F_{mJ}	$0.12987(36) \times 10^{-7}$
6 _{4,2}	$P_a^2 P_\alpha^4$	F_{mK}	$0.36055(57) \times 10^{-4}$
6 _{4,2}	$(1/2)\{P_a, P_b\} P_\alpha^4$	F_{mab}	$0.3193(70) \times 10^{-8}$
6 _{4,2}	$(1/2)\{P_a, P_c\} \sin 6\alpha$	D_{6ac}	$0.3022(82) \times 10^{-4}$
6 _{4,2}	$(1/2)\{P_b, P_c\} \sin 6\alpha$	D_{6bc}	$0.1206(12) \times 10^{-4}$
6 _{4,2}	$(1/2)\{P_a, P_c, P_a^2, \sin 3\alpha\}$	D_{3acm}	$-0.3795(11) \times 10^{-4}$
6 _{3,3}	$P^2 P_a P_\alpha^3$	ρ_{mJ}	$0.4567(12) \times 10^{-7}$
6 _{3,3}	$P_a^3 P_\alpha^3$	ρ_{mK}	$0.50072(62) \times 10^{-4}$
6 _{3,3}	$(1/2)\{P_a^2, P_b\} P_\alpha^3$	ρ_{mab}	$0.2957(67) \times 10^{-8}$
6 _{3,3}	$(1/2)\{P_a, P_b, P_c, P_\alpha, \sin 3\alpha\}$	ρ_{3bc}	$-0.26327(58) \times 10^{-4}$
6 _{2,4}	$P^4(1 - \cos 3\alpha)$	V_{3JJ}	$0.96440(90) \times 10^{-8}$
6 _{2,4}	$P^2 P_a^2(1 - \cos 3\alpha)$	V_{3JK}	$-0.38783(13) \times 10^{-6}$
6 _{2,4}	$P_a^4(1 - \cos 3\alpha)$	V_{3KK}	$0.43582(61) \times 10^{-6}$
6 _{2,4}	$P^2(P_b^2 - P_c^2)(1 - \cos 3\alpha)$	V_{3bcJ}	$0.33135(49) \times 10^{-8}$
6 _{2,4}	$(1/2)\{P_a^2, (P_b^2 - P_c^2)\}(1 - \cos 3\alpha)$	V_{3bcK}	$0.12328(30) \times 10^{-5}$
6 _{2,4}	$(1/2)P^2\{P_a, P_b\}(1 - \cos 3\alpha)$	V_{3abJ}	$0.786(13) \times 10^{-8}$
6 _{2,4}	$(1/2)\{P_a^3, P_b\}(1 - \cos 3\alpha)$	V_{3abK}	$-0.29046(69) \times 10^{-5}$
6 _{2,4}	$(1/2)(\{P_a, P_b^3\} - \{P_a, P_b, P_c^2\}) \cos 3\alpha$	V_{3abbc}	$0.21065(20) \times 10^{-6}$
6 _{2,4}	$P^4 P_\alpha^2$	F_{JJ}	$0.9587(98) \times 10^{-9}$
6 _{2,4}	$P^2 P_a^2 P_\alpha^2$	F_{JK}	$0.6039(15) \times 10^{-7}$
6 _{2,4}	$P_a^4 P_\alpha^2$	F_{KK}	$0.38758(38) \times 10^{-4}$

Table A.1. continued.

n_{lr}^a	Operator ^b	Par. ^c	Value ^{d,e}
6 _{2,4}	$(1/2)\{P_b^2, P_c^2\}P_a^2$	F_{b2c2}	$-0.4737(77) \times 10^{-8}$
6 _{2,4}	$(1/2)P^2\{P_a, P_c\} \sin 3\alpha$	D_{3acJ}	$-0.32666(10) \times 10^{-6}$
6 _{2,4}	$(1/2)\{P_a^3, P_c\} \sin 3\alpha$	D_{3acK}	$0.24680(74) \times 10^{-4}$
6 _{2,4}	$(1/2)P^2\{P_b, P_c\} \sin 3\alpha$	D_{3bcJ}	$-0.7458(16) \times 10^{-8}$
6 _{2,4}	$(1/2)\{P_a^2, P_b, P_c\} \sin 3\alpha$	D_{3bcK}	$-0.20601(44) \times 10^{-4}$
6 _{2,4}	$(1/2)(\{P_a, P_c^3\} - \{P_a, P_b^2, P_c\}) \sin 3\alpha$	D_{3acbc}	$0.26239(17) \times 10^{-6}$
6 _{2,4}	$(1/2)(\{P_b^3, P_c\} - \{P_b, P_c^3\}) \sin 3\alpha$	D_{3bcbc}	$-0.345(22) \times 10^{-8}$
6 _{1,5}	$P^4 P_a P_\alpha$	ρ_{JJ}	$0.9957(92) \times 10^{-9}$
6 _{1,5}	$P^2 P_a^3 P_\alpha$	ρ_{JK}	$0.36124(82) \times 10^{-7}$
6 _{1,5}	$P_a^5 P_\alpha$	ρ_{KK}	$0.15889(13) \times 10^{-4}$
6 _{1,5}	$(1/2)P^2\{P_a, (P_b^2 - P_c^2)\}P_\alpha$	ρ_{bcJ}	$0.3819(75) \times 10^{-9}$
6 _{1,5}	$(1/2)\{P_a, P_b^2, P_c^2\}P_\alpha$	ρ_{b2c2}	$-0.4311(73) \times 10^{-8}$
6 _{0,6}	P^6	Φ_J	$0.4568(18) \times 10^{-12}$
6 _{0,6}	$P^4 P_a^2$	Φ_{JK}	$0.13849(13) \times 10^{-9}$
6 _{0,6}	$P^2 P_a^4$	Φ_{KJ}	$0.8455(18) \times 10^{-8}$
6 _{0,6}	P_a^6	Φ_K	$0.26994(18) \times 10^{-5}$
6 _{0,6}	$P^4(P_b^2 - P_c^2)$	$2\phi_J$	$0.43864(71) \times 10^{-12}$
6 _{0,6}	$(1/2)P^2\{P_a^2, (P_b^2 - P_c^2)\}$	$2\phi_{JK}$	$0.3821(72) \times 10^{-9}$
6 _{0,6}	$(1/2)P^4\{P_a, P_b\}$	D_{abJJ}	$0.901(12) \times 10^{-12}$
8 _{8,0}	P_a^8	F_{mmm}	$0.4599(43) \times 10^{-9}$
8 _{7,1}	$P_a P_\alpha^7$	ρ_{mmm}	$0.1264(12) \times 10^{-8}$
8 _{6,2}	$P^2(1 - \cos 9\alpha)$	V_{9J}	$0.1612(37) \times 10^{-4}$
8 _{6,2}	$P_a^2(1 - \cos 9\alpha)$	V_{9K}	$0.293(14) \times 10^{-3}$
8 _{6,2}	$(P_b^2 - P_c^2)(1 - \cos 9\alpha)$	V_{9bc}	$0.4795(74) \times 10^{-5}$
8 _{6,2}	$P_a^2 P_\alpha^6$	F_{mmK}	$0.9527(87) \times 10^{-9}$
8 _{6,2}	$(1/2)\{P_a, P_c\} \sin 9\alpha$	D_{9ac}	$-0.764(24) \times 10^{-4}$
8 _{6,2}	$(1/2)\{P_a, P_c, P_a^2, \sin 6\alpha\}$	D_{6acm}	$0.478(13) \times 10^{-6}$
8 _{4,4}	$P^4(1 - \cos 6\alpha)$	V_{6JJ}	$0.6631(69) \times 10^{-9}$
8 _{4,4}	$P_a^4(1 - \cos 6\alpha)$	V_{6KK}	$-0.382(10) \times 10^{-7}$
8 _{4,4}	$P^2(P_b^2 - P_c^2)(1 - \cos 6\alpha)$	V_{6bcJ}	$0.11622(71) \times 10^{-8}$
8 _{4,4}	$(1/2)\{P_a^3, P_b\}(1 - \cos 6\alpha)$	V_{6abK}	$-0.432(11) \times 10^{-7}$
8 _{3,5}	$(1/2)\{P_a^3, P_b, P_c, P_\alpha, \sin 3\alpha\}$	ρ_{3bcK}	$0.1901(18) \times 10^{-8}$
8 _{2,6}	$P^6(1 - \cos 3\alpha)$	V_{3JJJ}	$-0.1652(40) \times 10^{-12}$
8 _{2,6}	$P^4 P_a^2(1 - \cos 3\alpha)$	V_{3JJK}	$0.7750(28) \times 10^{-11}$
8 _{2,6}	$P_a^6(1 - \cos 3\alpha)$	V_{3KKK}	$0.829(47) \times 10^{-10}$
8 _{2,6}	$P^4(P_b^2 - P_c^2)(1 - \cos 3\alpha)$	V_{3bcJJ}	$-0.2301(17) \times 10^{-12}$
8 _{2,6}	$(1/2)P^2\{P_a^2, (P_b^2 - P_c^2)\}(1 - \cos 3\alpha)$	V_{3bcJK}	$0.1481(89) \times 10^{-11}$
8 _{2,6}	$(1/2)P^2\{P_b^2, P_c^2\} \cos 3\alpha$	V_{3b2c2J}	$-0.756(32) \times 10^{-12}$
8 _{2,6}	$(1/2)(\{P_b^4, P_c^2\} - \{P_b^2, P_c^4\}) \cos 3\alpha$	$V_{3b2c2bc}$	$-0.22643(76) \times 10^{-11}$
8 _{2,6}	$(1/2)P^2(\{P_a, P_b^3\} - \{P_a, P_b, P_c^2\}) \cos 3\alpha$	V_{3abbcJ}	$-0.682(47) \times 10^{-12}$
8 _{2,6}	$P_a^6 P_\alpha^2$	F_{JJJ}	$0.5680(96) \times 10^{-15}$
8 _{2,6}	$P_a^6 P_\alpha^2$	F_{KKK}	$-0.5406(46) \times 10^{-9}$
8 _{2,6}	$P^4(P_b^2 - P_c^2)P_\alpha^2$	F_{bcJJ}	$-0.950(50) \times 10^{-15}$
8 _{2,6}	$(1/2)(\{P_b^4, P_c^2\} - \{P_b^2, P_c^4\})P_\alpha^2$	F_{b2c2bc}	$0.1125(40) \times 10^{-13}$
8 _{2,6}	$(1/2)P^4\{P_a, P_c\} \sin 3\alpha$	D_{3acJJ}	$0.4398(52) \times 10^{-11}$
8 _{2,6}	$(1/2)P^2\{P_a^3, P_c\} \sin 3\alpha$	D_{3acJK}	$0.1247(30) \times 10^{-10}$
8 _{2,6}	$(1/2)P^4\{P_b, P_c\} \sin 3\alpha$	D_{3bcJJ}	$0.10470(39) \times 10^{-11}$
8 _{2,6}	$(1/2)\{P_a^4, P_b, P_c\} \sin 3\alpha$	D_{3bcKK}	$0.1406(14) \times 10^{-8}$
8 _{2,6}	$(1/2)P^2(\{P_a, P_c^3\} - \{P_a, P_b^2, P_c\}) \sin 3\alpha$	D_{3acbcJ}	$-0.5366(44) \times 10^{-11}$
8 _{2,6}	$(1/2)P^2(\{P_b^3, P_c\} - \{P_b, P_c^3\}) \sin 3\alpha$	D_{3bcbcJ}	$0.3186(95) \times 10^{-12}$
8 _{2,6}	$(1/2)\{P_b^3, P_c^3\} \sin 3\alpha$	D_{3b3c3}	$-0.4538(18) \times 10^{-11}$
8 _{1,7}	$P_a^7 P_\alpha$	ρ_{KKK}	$-0.5405(45) \times 10^{-9}$
8 _{0,8}	P_a^8	L_K	$-0.1484(12) \times 10^{-9}$
10 _{8,2}	$(1/2)\{P_a, P_c, P_a^2, \sin 9\alpha\}$	D_{9acm}	$-0.662(23) \times 10^{-6}$
10 _{6,4}	$(1/2)\{P_a^2, (P_b^2 - P_c^2)\}(1 - \cos 9\alpha)$	V_{9bcK}	$-0.4026(56) \times 10^{-7}$
10 _{4,6}	$P_a^6(1 - \cos 6\alpha)$	V_{6KKK}	$-0.885(51) \times 10^{-10}$
10 _{4,6}	$(1/2)P^4\{P_a, P_c\} \sin 6\alpha$	D_{6acJJ}	$-0.1390(70) \times 10^{-11}$

Table A.1. continued.

n_{tr}^a	Operator ^b	Par. ^c	Value ^{d,e}
10 _{4,6}	$(1/2)P^2\{P_a^2, P_b, P_c\} \sin 6\alpha$	D_{6bcJK}	$-0.1579(29) \times 10^{-10}$
10 _{4,6}	$(1/2)P^2(\{P_a, P_c^3\} - \{P_a, P_b^2, P_c\}) \sin 6\alpha$	D_{6abcJ}	$0.595(13) \times 10^{-11}$
10 _{2,8}	$P_a^8(1 - \cos 3\alpha)$	V_{3KKKK}	$-0.217(15) \times 10^{-12}$
10 _{2,8}	$(1/2)(\{P_b^6, P_c^2\} + \{P_b^2, P_c^6\}) \cos 3\alpha$	$V_{3b6c2b2c6}$	$0.304(18) \times 10^{-16}$
12 _{4,8}	$P_a^8(1 - \cos 6\alpha)$	V_{6KKKK}	$0.222(17) \times 10^{-12}$

Notes. ^a $n=t+r$, where n is the total order of the operator, t is the order of the torsional part and r is the order of the rotational part, respectively. The ordering scheme of Nakagawa et al. (1987) is used. ^b $\{A, B, C, D, E\} = ABCDE + EDCBA$. $\{A, B, C, D\} = ABCD + DCBA$. $\{A, B, C\} = ABC + CBA$. $\{A, B\} = AB + BA$. The product of the operator in the second column of a given row and the parameter in the third column of that row gives the term actually used in the torsion-rotation Hamiltonian of the program, except for F , ρ and A_{RAM} , which occur in the Hamiltonian in the form $F(p_a + \rho P_a)^2 + A_{\text{RAM}} P_a^2$. ^c The parameter nomenclature is based on the subscript procedure of Xu et al. (2008). ^d Values of the parameters in units of cm^{-1} , except for ρ , which is unitless. ^e Statistical uncertainties are given in parentheses as one standard uncertainty in units of the last digits.